Case Studies in Construction Materials 23 (2025) e05427

Contents lists available at ScienceDirect

Case Studies in Construction Materials

journal homepage: www.elsevier.com/locate/cscm

Full length article

Influence of thermally activated industrial concrete fines of different origin on mortar strength development

Jan P. Höffgen *, Sebastian Bruckschlögl, Bernhard Wetz, Frank Dehn

Karlsruhe Institute of Technology (KIT), Institute for Concrete Structures and Building Materials (IMB), Gotthard-Franz-Str. 3, Karlsruhe, 76131, Germany

ARTICLE INFO

Keywords:
Concrete
Cement
Construction waste
Recycling
Thermal activation
Supplementary cementitious material

ABSTRACT

Thermal activation of recycled concrete fines (RCFs) has gained traction as a promising method for mineral waste recycling and the substitution of Portland cement, thereby reducing CO_2 emissions. However, as the composition of concrete fines varies, their performance as supplementary cementitious materials (SCMs) also changes. The present work compares 25 industrial concrete fines from various sources and compositions concerning their thermal decomposition and their influence on hydration heat and mortar compressive strength development. RCFs were processed at 100 °C, 400 °C, and 600 °C, and tested for their hydration heat development and compressive strength. Findings show that blended cements exhibit fast rehydration, which results in high early strength. Compressive strength of mortar containing processed RCFs increases with activation temperature. However, the mass loss from the disintegration of hydraulic hardened cement paste phases is a more significant parameter for assessing the strength contribution. Based on these findings, the study presents a new model for predicting compressive strength alongside current provisions for established SCMs. While compressive strength contribution of RCFs processed at 100 °C on average assumes about 10 % of CEM I reactivity and may be even negative, the same RCFs show an in increase to 41 % for 600 °C, with some RCFs even exceeding 60 %. This allows for the substitution of increasingly scarce fly ash, which exhibits strength contribution around 40 %-50 %.

1. Introduction

The production of cement is one of the most significant contributors to climate change, accounting for 8 % of global CO_2-emissions [1]. Emissions are attributed to two major sources: fossil fuels required for cement clinker processing temperatures up to 1450 °C and the calcination of carbonates from clinker raw meal. While the former can be abated through alternative fuels, the latter requires a switch to carbon-free calcitic feedstocks [2,3].

The hardening process of ordinary Portland cement (OPC, or CEM I according to EN 197-1:2011) based concrete relies on the hydraulic reaction of cement clinker, which forms high amounts of calcium-silicate-hydrates (C-S-H) responsible for strength development, and calcium hydroxide for high alkalinity from the hydration of alite (C_3S) and belite (C_2S), as well as hydration products of aluminous and ferrous clinker phases [4,5].

For ecological reasons, clinker can be partially substituted through alternative binders, so-called supplementary cementitious materials (SCMs), such as limestone powder, ground granulated blast-furnace slag (GGBS), amorphous silica, or fly ash [5–10]. These exhibit a different, in general lower, reactivity (compared to OPC) [3,11–13]. This depends on their mineralogical and chemical

* Corresponding author.
E-mail address: jan.hoeffgen@kit.edu (J.P. Höffgen).

https://doi.org/10.1016/j.cscm.2025.e05427
Received 23 July 2025; Received in revised form 18 September 2025; Accepted 13 October 2025
Available online 16 October 2025

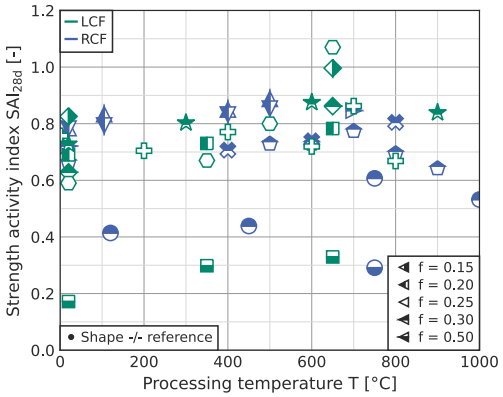

Fig. 1. Strength activity indices (SAI) over processing temperatures for different concrete fines and substitution rates (f) from various exemplary references.
LCF: fines from laboratory-made concrete, RCF: fines from concrete recycling plants.
Marker shapes: ⬠: [73], △, ▽: [58], ▷: [74], ○: [49], ×: [75], □: [76], ◇: [54], ⬡: [77], +: [66], ★: [71].

composition, where SCMs may react with hydration products from the OPC reaction, or are inert. Facing the high demand for sustainable building materials, research focuses on identifying potential SCMs [7,14].

Among these, recycled concrete fines (RCFs) are particularly promising [15–19]. Their application is identified as closed circularity, especially since the use as fine concrete aggregates is impeded through their high porosity and water absorption, which results in weak concrete performance [20,21]. This is associated with the enrichment of hardened cement paste (HCP) with decreasing particle size during mechanical processing of recycled concrete aggregates [22]. Alternatively, RCFs can be ground and serve as SCMs, where they act as fillers and nuclei for the hydration of OPC [23–25]. However, material properties can be enhanced by thermal activation. HCP dehydrates at elevated temperatures: Calcium silicate hydrates (C-S-H) start to decompose at 110 °C [26]. The upper limit of C-S-H decomposition lies between 300 °C and 500 °C [26–28]. Calcium hydroxide disintegrates in a smaller range between 400 °C and 550 °C [26,27,29]. Aluminous hydration products are anhydrous at temperatures higher than 400 °C [27,30–34]. Favored by the lower processing temperatures compared to clinker production, this process can be almost emission-free, as long as fossil fuels are avoided in favor of renewable energy [35–39]. Only when processing temperature exceeds 650 °C, carbonates start to disintegrate with the subsequent emission of CO_2. Dehydrated cement paste (DCP) is a reactive SCM: dehydrated C-S-H forms different variations of $\alpha' C_2S$ with C/S-ratio between 1.73 and 1.90 [4,40–47]. C-S-H from the rehydration of $\alpha' C_2S$ mainly forms within the porous structure of DCP-particles, resulting in a loose microstructure with weak interparticle connectivity [46,48,49]. However, when used as a partial Portland cement substitute, the water uptake and consumption in the DCP-pores reduce the water available for clinker hydration, which subsequently enhances the strength of the surrounding matrix [27,50–52]. The rehydration of $\alpha' C_2S$ exhibits a high velocity, more so when free lime from disintegrated calcium hydroxide or calcium carbonates is present in the DCP. This results in an accelerated hydration with high initial hydration heat release and high early strength development [27,28,40,43,46,50,52,53]. DCP can replace up to 40 wt% of OPC with no significant negative impact on compressive strength [45,52,54–60]. Optimum processing temperatures mostly lie within the range of 350 °C–800 °C [43,49,56,60–69]. Higher temperatures induce the reformation of $\alpha' C_2S$ to less reactive phases [43,46,51,68].

However, besides HCP, RCFs consist of fine natural aggregates, which are mostly inert after processing below calcination temperature (> 650 °C, depending on mineral composition) [70,71]. Inert aggregates in dehydrated concrete fines mostly exhibit no strength contribution aside from the nucleation and filler effect [49]. However, natural aggregates may contain amorphous siliceous or other pozzolanic phases [72]. Aside from different aggregate compositions and matrix porosity, RCFs vary in terms of the chemical composition of the original cement and SCMs used for the production of the source concrete.

For the assessment of the strength contribution of SCMs, the strength activity index (SAI) provides a single-point direct quantification method. SAI_t is defined through Eq. (1) as the relative compressive strength f_c of a reference mortar (or concrete) with OPC and a SCM-mortar with partial OPC substitution at a given age t. Requirements for mix composition and SAI-thresholds depend on individual SCM standards: European standard EN 15167-1:2006 requires $SAI_{7\,d} \geq 0.45$ and $SAI_{28\,d} \geq 0.70$ for standard mortar containing 50 wt% GGBS, and EN 450-1:2012 defines thresholds of $SAI_{28\,d} \geq 0.75$ and $SAI_{90\,d} \geq 0.85$ for a substitution rate of 25 wt% through fly ash.

$$SAI_t = \frac{f_{c,SCM,t}}{f_{c,ref,t}} \tag{1}$$

$SAI_{28\,d}$ for thermally activated concrete fines mostly lie within a range, which fulfills the aforementioned requirements for fly ash. However, the literature data presented in Fig. 1 also shows a great variation between results from different publications, where, besides concrete fines composition, different processing and testing approaches may negatively affect the comparability of these results.

Table 1
Overview of the investigated parameter combinations and processing temperatures for different precursors. RCF: Recycled concrete fines, RCA: Recycled concrete aggregates, FCR: Fresh concrete recycling, F: Filter cake.

Marker	Precursor		Variants		100 °C	400 °C	600 °C
□	RCF	0/2 mm	A1-	0/0.125 s	×		×
				0/0.25 s			×
				0/0.25	×		×
				0/0.5	×		×
				0/1	×		×
				0/2	×		×
◇	RCF	0/2 mm	A2-	0/0.25			×
				0/2			×
△	RCF	0/2 mm	B1-	0/0.25	×	×	×
				0/0.5	×		×
				0/1	×		×
				0/2	×	×	×
▽	RCA	0/45 mm	B2-	0/0.25	×		×
				0/2	×		×
▷	RCA	0/45 mm	C-	0/0.25	×		×
				0/2	×		×
○	RCA	0/16 mm	D-	0/0.25	×		×
				0/2	×	×	×
	FCR	F		F	×	×	×
×	RCF	0/2 mm	E-	0/0.25	×		×
				0/2	×		×
+	RCF	0/3 mm	F-	0/0.25	×		×
				0/2	×	×	×
⬠	RCF	F	G-	F	×	×	×
⬡	FCR	F	H-	F	×		×

Ultimately, for these variations, the present data is insufficient for providing a means for predicting compressive strength of mortar or concrete containing thermally processed RCFs. Besides the impact of different experimental procedures, the influence of varying RCF composition itself has rarely been investigated in the literature, where most studies focus on evaluating a single RCF. For the industrial application of thermally processed RCFs as SCMs, knowledge about fluctuating material properties is paramount. A direct comparison of the strength contribution of RCFs from different sources, and subsequently, a model for predicting compressive strength based on RCF properties, is lacking. Therefore, the present study investigates the influence of thermally activated RCFs of different compositions on compressive strength with the ultimate objective of providing a comprehensive model for predicting compressive strength of mortar or concrete containing therally processed RCFs as SCM.

2. Experimental program

The experimental program comprises two distinct goals: The first step is to analyze parameters of the thermal activation, followed by the evaluation of thermally activated concrete fines as supplementary cementitious materials (SCM) in comparison to ground granulated blast-furnace slag, black coal fly ash, and limestone powder as established concrete binders.

2.1. Materials

The experimental assessment uses and compares eleven different batches of waste concrete from eight different processing plants (labeled A – H). From two plants (A and B), two batches produced several months apart were procured. For batches of recycled concrete aggregates (RCA), where the maximum particle size exceeded 2 mm, larger particles were removed through dry-sieving before any further handling. In addition to the variant "0/2" [mm] from each recycled concrete fines (RCF) batch, an additional variant "0/0.25" [mm] was produced through a second dry-sieving step. From two batches, additional variants with different particle sizes were obtained in a similar procedure. Three batches had a different preprocessing: Batch G-F originated from a mineral waste processing plant, which used a wet-separation, where concrete fines smaller than 100 µm, rather than the typical 2 mm from the other batches, can be obtained as residue filter-cake (F). In contrast, D-F and H-F denote filter cakes from two fresh-concrete recycling (FCR) plants. Following the subsequent thermal activation, concrete fines were ground to a maximum particle size of 125 µm, except for the variants A1-0/0.125s and A1-0.25s, which were left without grinding after thermal processing ("s"). Activation temperature was 400 °C or 600 °C, as hereinafter indicated through suffices "–400" and "–600". Additionally, concrete fines were dried at 105 °C and ground (suffix "–100"). Table 1 gives an overview of the, in total, 25 different concrete fines variations and 53 processed concrete fines combinations.

Besides concrete fines, the experimental analyses used OPC (CEM I 42.5 R, "CEM I") as base binder and ground granulated blast-furnace slag ("S"), fly ash ("FA"), as well as limestone powder ("L") as established SCMs for reference. Additionally, siliceous river sand (0/2 mm, "RS") served as fine aggregates.

CEM I was also used to produce an artificial hardened cement paste ("CEM") with a water-cement ratio of $w/c = 0.5$, which was used for the evaluation of thermal activation processing parameters. CEM was kept moist for 9 months, before drying at 105 °C and subsequent grinding ("CEM-100").

2.2. Experimental procedures

Initially, all materials, including thermally activated fines, were characterized for their chemical composition as well as their density and particle size distribution. Concrete fines were also investigated through thermogravimetric analyses before and after activation, using sample sizes of 160 mg and a heating rate of 10 K/min.

The evaluation of thermal activation processing parameters followed a three-step approach. First, the base material CEM-100 was examined for its thermal behavior in the same thermogravimetric test setup, but with varying heating rates (1 K/min, 5 K/min and 10 K/min) and sample sizes of 5 g. The test at 10 K/min was repeated in a different setup with a sample size of 60 mg, which included a mass spectrometer for measuring ion currents (IC) of H_2O and CO_2. The second step exploited the versatility of the thermogravimetric setup for processing CEM-100 at varying temperatures, heating and (passive) cooling rates, as well as holding times. Finally, the influence of varying sample sizes and holding times was analyzed with the ultimate goal of defining the thermal processing regimen for the subsequent RCF activation.

CEM I, reference SCMs, and select activated concrete fines were used for isothermal hydration heat measurements at 20 °C with internal mixing, which allowed the determination of the initial heat release. Following preliminary tests on mixing efficiency and homogeneity, the water-binder ratio was set to $w/b = 0.6$ for all materials. SCMs were investigated in combination with CEM I and a substitution rate of $f = 0.3$. For all mixes, a double determination was carried out, except for the base mix with pure CEM I, which consisted of eight single measurements.

Strength development tests used a mortar with 50 v% quartzitic river sand (0 mm-2 mm) as aggregates. For the assessment of SCM influence, from all SCMs two mixes with $w/b = 0.4$ and $w/b = 0.5$ at $f = 0.3$ were produced, with selected SCMs adding $w/b = 0.5$ at $f = 0.1$, and $f = 0.5$. Fourteen base mixes with pure CEM I used $w/b = 0.40$–0.65, which were produced in three series repeated over the experimental program. In case of stiff mortars, superplasticiser was added to ensure comparable workability. After mixing, mortar was placed in steel molds, which were moist-cured for 1 d, and, following demolding, stored under water at 20 °C. Strength testing used three prisms ($(20 \times 20 \times 80)\,mm^3$) at 2 d and 28 d. Since thermal activation and grinding of concrete fines was a resource-intensive process, this smaller specimen size was chosen, compared to standard mortar bars ($(40 \times 40 \times 160)\,mm^3$), to reduce the amount of binder required for each mix. First, flexural strength f_f was determined with a span of 50 mm at a loading rate of $\dot{f}_f = 10$ N/s. Compressive strength (f_c) testing used six prism halves at a loading rate of $\dot{f}_c = 600$ N/s.

Fig. A.14 in the appendix section gives a graphical illustration of the experimental procedures.

3. Results and discussion

3.1. Thermal activation parameters

The temperature-dependent mass loss (Δm) of CEM-100 in Fig. 2 shows the aforementioned segments, although all measurements produce unique results. With decreasing heating rate, decomposition processes occur at lower temperatures, resulting in increased mass losses at the same temperatures. In particular, the decomposition of calcium hydroxide shows a strong influence of the heating rate, with an offset of more than 50 K. This offset is interrelated with sample size, as with larger sizes, thermal conduction impedes a uniform temperature within the sample. Accordingly, Δm in the thermogravimetric measurement coupled with mass spectroscopy, which used a sample size of 60 mg and a heating rate of 10 K/min, is closest to Δm at 1 K/min and 5 g. Similar observations are made for the decomposition of carbonates, which starts at 550 °C and peaks at 720 °C, but is offset to higher temperatures for larger sample sizes.

Conversely, Fig. 2 allows for the determination of processing temperatures that are less susceptible to heating rate and/or sample size, thus enabling better reproducibility and comparability across different thermal processing setups. Subsequently, a processing temperature of 600 °C was chosen for the following analyses. Additionally, at 600 °C mass spectroscopy shows an almost complete loss of H_2O, while CO_2 emissions are still low.

In addition to the processing temperature of 600 °C, two other processing temperatures were identified from Fig. 2. At a temperature of 400 °C, apart from the decomposition of calcium hydroxide, the majority of the dehydration is complete. At a temperature of 800 °C, a high proportion of the carbonates in the cement paste is also decomposed. In combination with 600 °C, 400 °C, and 800 °C allow for evaluating the influence of calcium hydroxide and carbonates decomposition.

To investigate this preselection of processing temperatures in more detail, samples of CEM-100, each weighing 5 g, were activated in the same thermogravimetric setup. In particular, the different holding times, heating, and cooling rates allowed the influence of system inertia and thus control accuracy to be addressed. The core parameter combination was 5-600-0-10, which is an abbreviation for a heating rate of 5 K/min, target temperature of 600 °C, holding time of 0 h, and an initial cooling rate of 10 K/min. Parameter variations combine heating rates of 1 K/min, 5 K/min and 10 K/min, holding times of 0 h and 2 h and initial cooling rates of 5 K/min, 10 K/min and 20 K/min. The latter could not be actively controlled, but denotes the maximum rates during passive cooling.

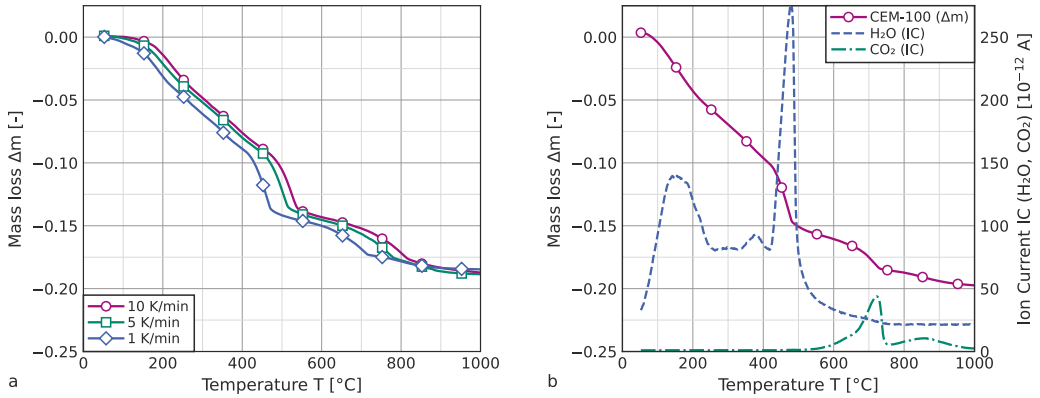

Fig. 2. Temperature-dependent mass loss of CEM-100. a: influence of different heating rates (sample size 5 g), b: additional ion current measurements at a heating rate of 10 K/min (sample size 60 mg).

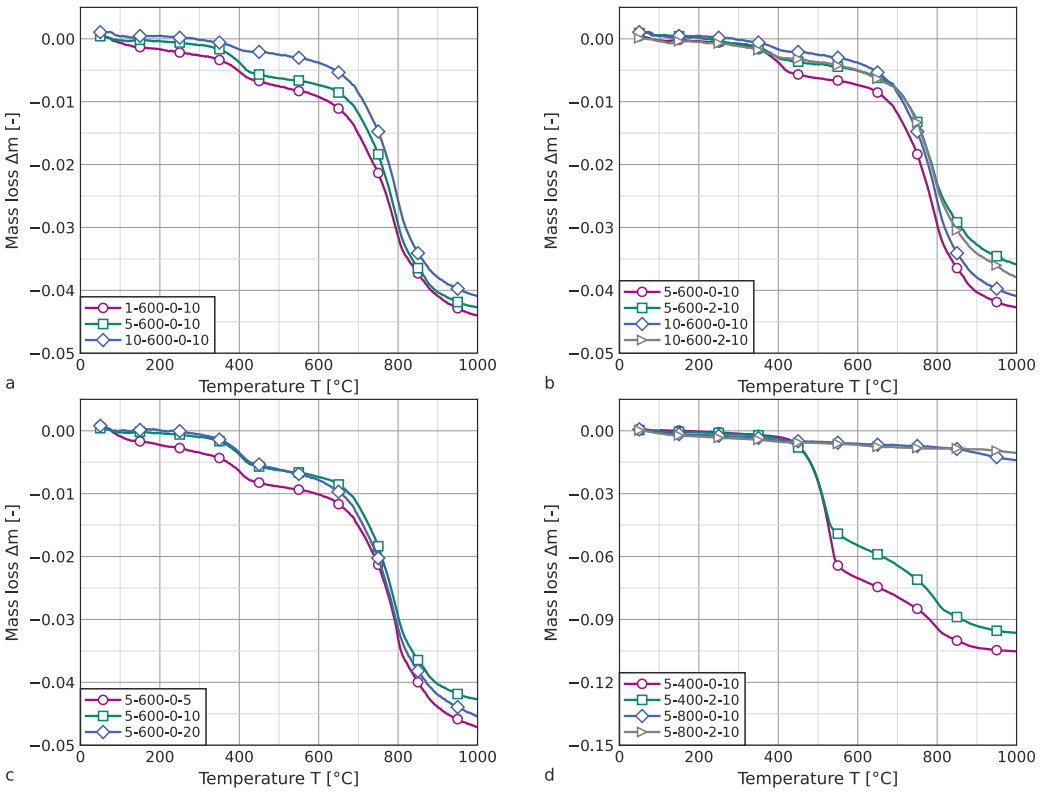

Fig. 3. Thermogravimetric analysis of CEM-100 activated at different processing parameters.

Additionally, for processing temperatures of 400 °C and 800 °C, the influence of different holding times (0 h and 2 h) was evaluated at a heating rate of 5 K/min and a cooling rate of 10 K/min.

From these samples, subsamples were taken and initially characterized in a repeated thermogravimetric investigation. For this purpose, sample masses of 160 mg were examined at a heating rate of 10 K/min. Fig. 3 shows the resulting mass losses as a function of temperature up to 1100 °C.

In an ideal thermal preparation, it would be expected that the curve progressions remain constant until the preparation temperature is reached again and only then show a mass loss with increasing temperature. Fig. 3 shows that this is not the case for any of the samples prepared at 600 °C – all samples show varying degrees of mass loss. However, no systematic influence of the processing parameters can be identified. An increased mass loss occurs at approximately 400 °C, while the decomposition of calcium hydroxide is complete in all cases at around 500 °C. This shift in the decomposition temperature suggests that the observed

mass losses are due to compounds formed after thermal processing (compare [43,78,79]). A probable reason is that the hot samples cannot be immediately removed from the test device after processing. At the same time, the results underscore the importance of rapid further processing of the samples.

The processing temperatures of 400 °C and 800 °C were only considered concerning different holding times. Here, it is shown that processing at 800 °C, in contrast to processing at 600 °C, results in very low mass losses for both parameter combinations during the repeated thermogravimetric measurements. Both samples prepared at 400 °C also show only a slight mass loss up to the previous preparation temperature. However, a plausible influence of the treatment duration is evident: A temperature of 400 °C is not sufficient to decompose calcium hydroxide. However, an extension of the processing duration can have a similar effect as a reduction of the heating rate (see Fig. 2), so that a small amount of calcium hydroxide is decomposed after a duration of 2 h. Similar, albeit less pronounced, observations can be made for the samples processed at 800 °C.

In the third step of the analysis of processing parameters, CEM-100 was activated in different crucibles for either 3 h or 6 h in a static high-temperature furnace. The target temperature was 600 °C, with a heating rate of 5 K/min. Finally, the results from the static furnace were compared to the activation in a rotary furnace. In contrast to processing in crucibles, a rotary furnace continuously agitates the sample, resulting in a homogeneous temperature distribution. Holding time was therefore reduced to 0 h and 1 h. Immediately after the preset test duration ended, the static furnace opened automatically, and the samples were cooled in their covered crucibles at a laboratory climate before storage in desiccators. The samples in the rotary furnace were cooled in their containers at laboratory climate and stored in desiccators after reaching a temperature of < 200 °C.

Subsequently, thermogravimetric measurements were carried out on subsamples, which are shown in Fig. 4. The measurements illustrate a mutual influence between crucible size and preparation duration: While small crucibles already show similarly successful preparation after 3 h as the samples in Fig. 3, larger samples (examined were 0.75 kg and 1.0 kg) show a significantly increased mass loss between 400 °C and 600 °C, suggesting that the samples were not heated homogenously. Consequently, longer preparation times are required for larger samples. However, 6 h proved sufficient for all sample sizes up to 1.5 kg. The rotary furnace allows for a strongly reduced holding time. It is evident that the sample, where the heat treatment was terminated immediately after reaching the target temperature of 600 °C (0 h), subsequently showed the lowest mass loss below 600 °C. Extending the preparation by 1 h brought no additional benefit, with the mass loss subsequently slightly increased. An influence of storage can be assumed here, analogous to the previous experiments in the static furnace. The deviation between the two samples from the rotary furnace is smaller than the deviation between the two repeated samples from the static furnace. All samples show different mass losses above 700 °C, with no systematic pattern evident.

Subsequently, the procedure where RCFs were treated for 6 h in a static furnace at the target temperature following a heating ramp at 5 K/min was elected for the main analyses.

3.2. Precursors characterization

Fig. 5 presents the chemical compositions of RCFs (sieved to 2 mm and 0.25 mm) measured by WDXRF, the corresponding filter cakes, as well as CEM I, reference SCMs, and siliceous river sand (RS). It becomes apparent that the examined RCFs contain a similarly low amount of Al_2O_3 and Fe_2O_3. In contrast, RCFs contain high amounts of SiO_2, indicating the presence of siliceous aggregates. CaO- and MgO-content, on the other hand, increases with decreasing particle size, thus implying the concentration of hydrated cement in smaller particles.

Fig. 6 shows the mass loss of selected RCFs before thermal processing. The finer materials generally exhibit greater mass losses than the corresponding variants with a maximum grain size of 2 mm. However, the difference does not follow any apparent systematics and varies in magnitude for individual RCFs. The highest mass loss at 600 °C is observed for the RCF “D-F”, a filter cake from fresh concrete recycling. None of the examined samples shows an increased mass loss at around 500 °C, which would be associated with the decomposition of calcium hydroxide. It can therefore be assumed that calcium hydroxide has been converted to other compounds such as $CaCO_3$ through natural carbonation. Regarding the mass losses between 650 °C and 850 °C, which are associated with the decomposition of carbonates, the samples also show significant differences among each other. The RCFs from plant A and the filter cake from plant G show the highest mass losses here, while RCFs from plant D show only slight mass losses, which also end at lower temperatures of around 800 °C. This, in conjunction with the WDXRF results, which indicate a high CaO-content in RCFs from plants A and G, suggests that the RCFs contain different primary aggregates with varying calcium carbonate contents and variations.

The particle size distribution of processed RCFs shows a generally good comparability between different samples, except processed filter cakes (see Table 2). The latter exhibits smaller particle sizes, which are similar to limestone powder. Processing at 600 °C before grinding has a minor effect on the particle size distribution.

3.3. Concrete fines performance as SCM

3.3.1. Hydration heat

The hydration heat flow calorimetry measurements were limited to CEM I, S, FA, L, and selected RCFs processed at 600 °C. Fig. 7 includes the span obtained from eight single measurements, as well as the average of the double determinations performed for all measurements, where 30 wt% of CEM I was substituted through SCMs. The released hydration heat in Fig. 7 shows a great similarity between the processed RCFs and a great similarity to the mixture of CEM I with blast-furnace slag, exceeding the values for fly ash and limestone powder. Additionally, the heat release of finer raw materials (0/0.25 mm) is slightly increased compared to coarser

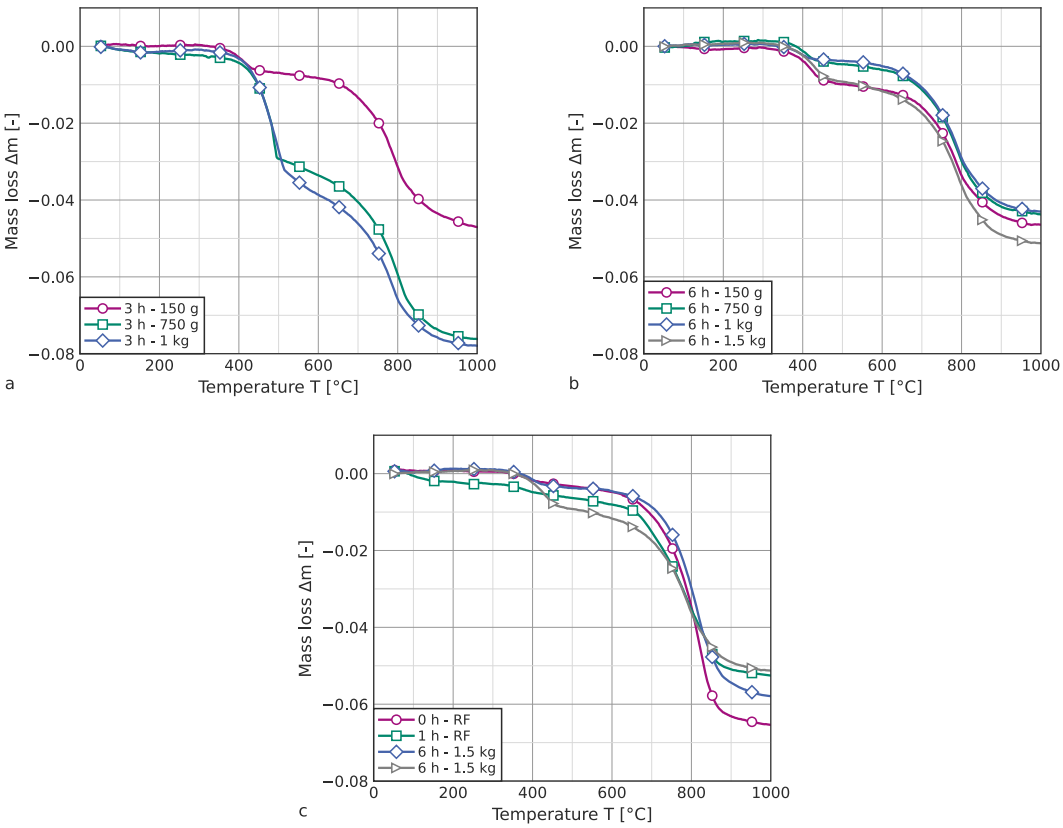

Fig. 4. Thermogravimetric analysis of CEM-100 activated in a static furnace with different sample sizes and holding times (a: 3 h, b: 6 h) and a rotary furnace "RF" (c).

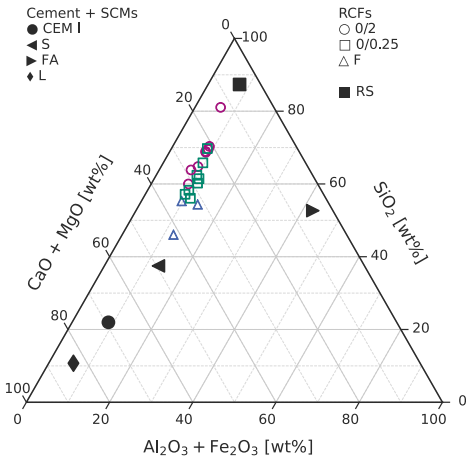

Fig. 5. Relative chemical composition of base materials and recycled concrete fines (RCF) through WDXRF (see tabulated data in the appendix section Table A.5).

raw materials (0/2 mm). Noteworthy is the hydration heat release of D-F (filter cake from a fresh concrete recycling plant). Here, a significantly increased heat release is evident in the first minutes after water addition. Additionally, the subsequent local maximum

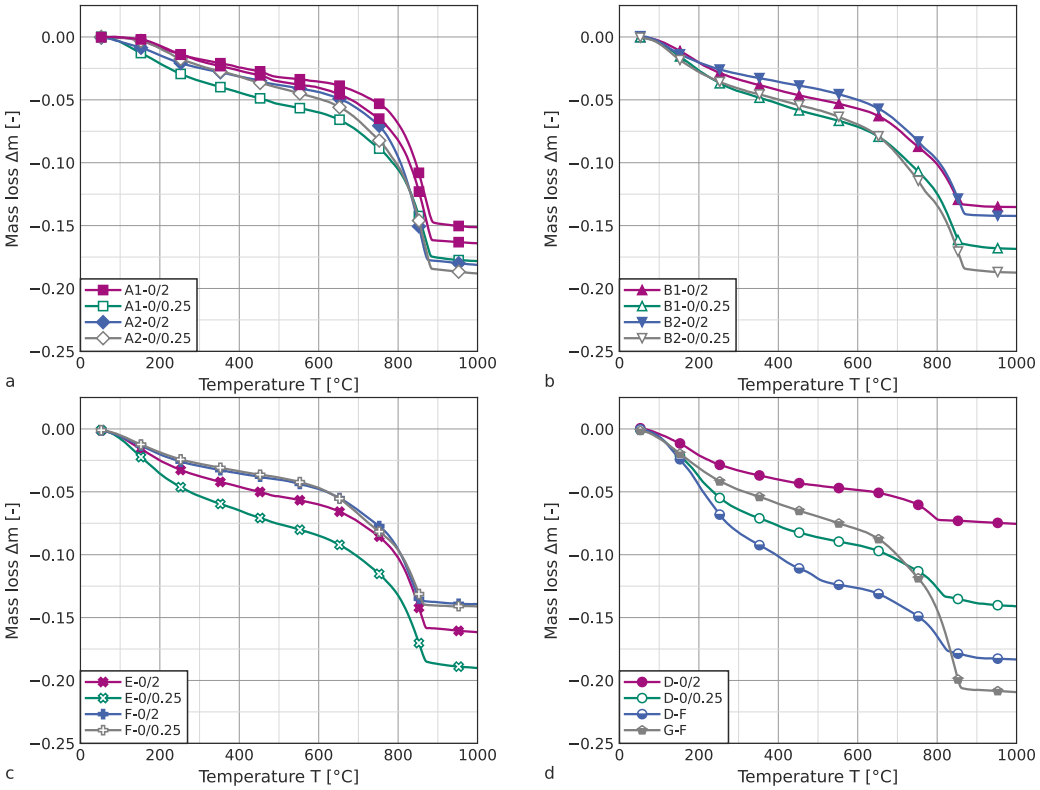

Fig. 6. Thermogravimetric characterization of select RCFs (sample size 160 mg, heating rate 10 K/min).

Table 2
Relevant characteristics (average and standard deviation at 10 v%, 50 v%, and 90 v% passing) of the particle size distribution of processed concrete fines and reference binders. Results only include values where pairs of RCFs were processed at both 100 °C and 600 °C.

	Qty.	d_{10} [µm]	d_{50} [µm]	d_{90} [µm]
CEM I	1	1.7	12.1	32.9
S	1	2.1	12.3	30.0
FA	1	2.9	21.6	83.4
L	1	1.9	12.5	44.4
0/2–100	7	1.8(3)	13.2(33)	54.1(83)
0/2–600		1.8(3)	14.1(33)	57.1(71)
0/0.25–100	7	1.8(3)	13.7(23)	55.2(58)
0/0.25–600		1.8(2)	14.0(16)	57.7(52)
F-100	3	2.2(6)	11.6(27)	44.7(109)
F-600		2.1(4)	10.1(13)	41.6(18)

of the hydration heat flow is lower and occurs earlier. However, the following decline in heat release is reduced, so this sample ultimately shows the highest heat release of all investigated mixtures of CEM I and processed RCFs.

3.3.2. Compressive strength development

The influence of cement, and SCMs, on compressive strength development can be characterized through the ratio of 2 d- to 28 d-strength (r_2). Fig. 8 shows results for the strength ratio r_2 for mortar with CEM I at different w/c-ratios and the partial replacement of CEM I through latent-hydraulic blast-furnace slag (S), pozzolanic fly ash (FA), or limestone powder (L). Particularly for CEM I, but also for mortar with SCMs, strength development accelerates with higher 28 d-compressive strength, i.e., for lower w/c-ratio and lower substitution rate through SCMs. Correspondingly, with the same strength, the partial substitution of CEM I through blast-furnace slag or fly ash leads to reduced strength at the age of 2 d. r_2 for these mixtures ranges from 0.4 to 0.5. The replacement of CEM I with inert limestone powder has the greatest impact on mortar compressive strength compared to blast-furnace slag or fly ash. Apart from that, the strength ratio r_2 is not additionally affected. Mixtures with CEM I and limestone powder, as well as

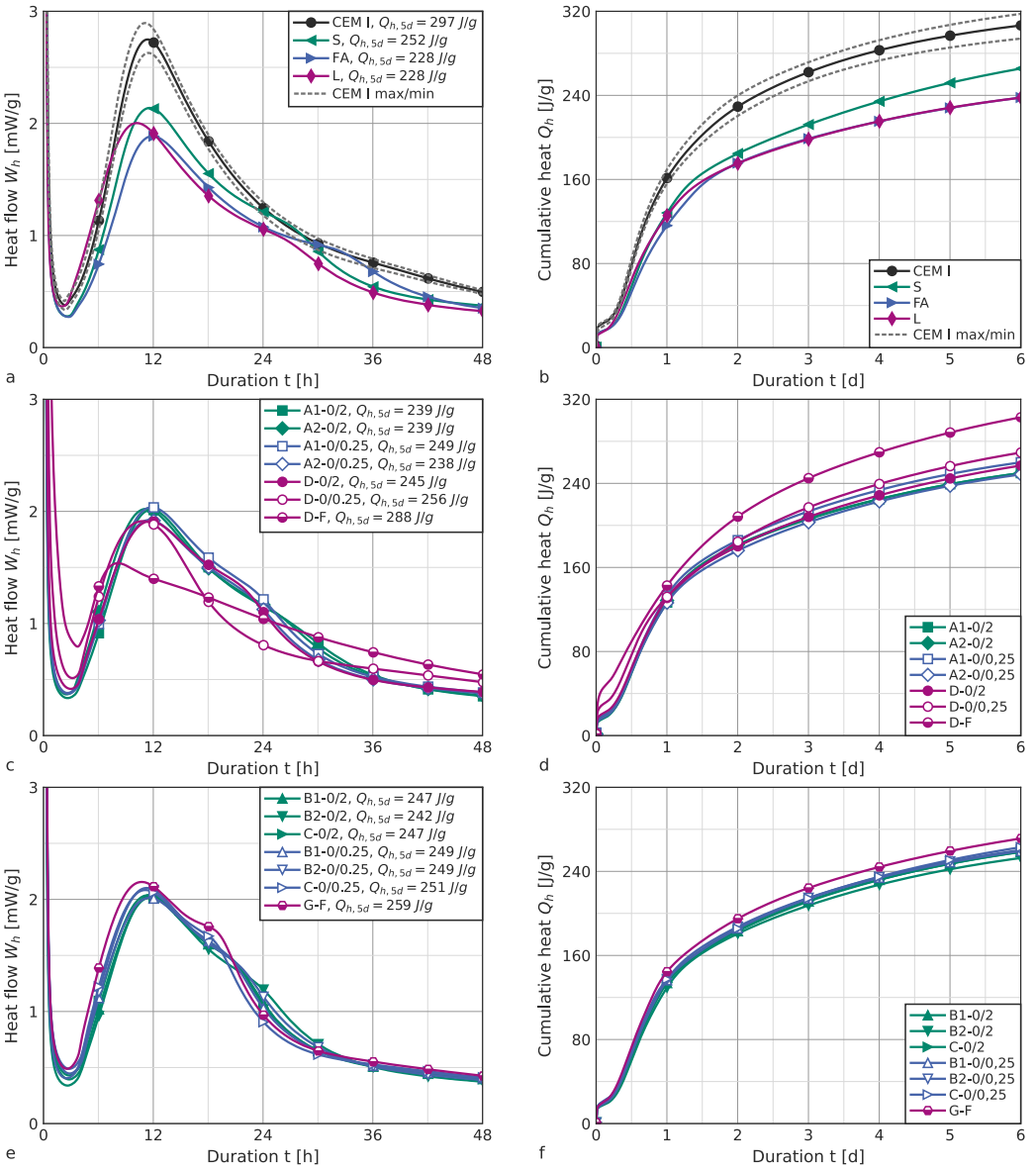

Fig. 7. Hydration heat of CEM I, including standard deviation, and mixtures of 70 wt% CEM I and 30 wt% reference SCMs, or RCFs processed at 600 °C.

mixtures with pure CEM I, show strength-dependent values of r_2 in the range of 0.5 to 0.7. With the same strength at the age of 28 d, these mixtures tend to have higher 2 d compressive strength than mixtures with fly ash or blast-furnace slag.

The compressive strength development of mixtures with thermally activated RCFs shows similar r_2 values to the pure CEM I mixtures, with even higher r_2 values up to 0.7 being achieved at the same 28 d compressive strength — regardless of the processing temperature. This indicates an accelerating effect of RCF on compressive strength development.

3.3.3. Compressive strength at 28 d

The assessment of compressive strength at a mortar age of 28 d uses both strength activity indices as well as the *k*-value approach.

Strength activity indices ($SAI_{28\,d}$) for processed concrete fines replacing 30 wt% of CEM I were calculated based on the average $f_{c,ref,28\,d}$ = 53.3 MPa. Results indicate a temperature dependence, with average $SAI_{28\,d}(100\,°C)$ = 0.64(7) and $SAI_{28\,d}(600\,°C)$ = 0.74(5). Fig. 9 illustrates individual results for different concrete fines variations. For comparison, the double determination of SAI for established SCMs yield $SAI_{28\,d}(S)$ = 0.91 for slag, $SAI_{28\,d}(FA)$ = 0.78 for fly ash, and $SAI_{28\,d}(L)$ = 0.66 for limestone powder.

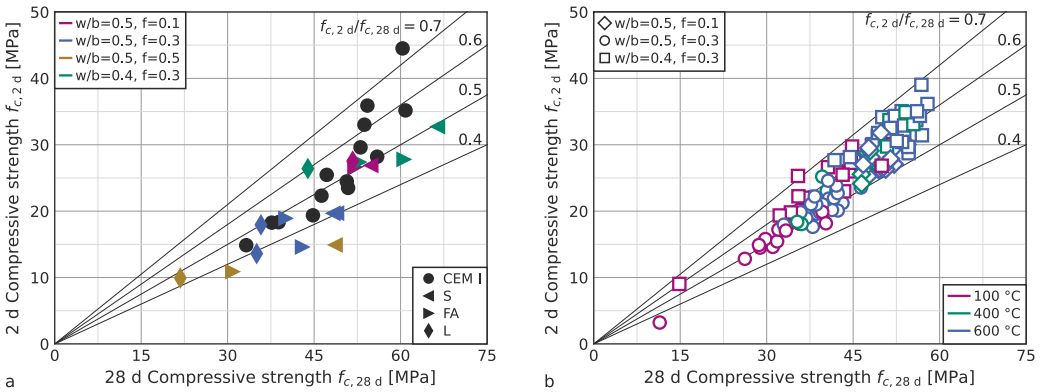

Fig. 8. Mortar compressive strength f_c at an age of 2 d over 28 d for different mix designs and CEM I substitution through reference SCMs (a) or processed concrete fines (b).

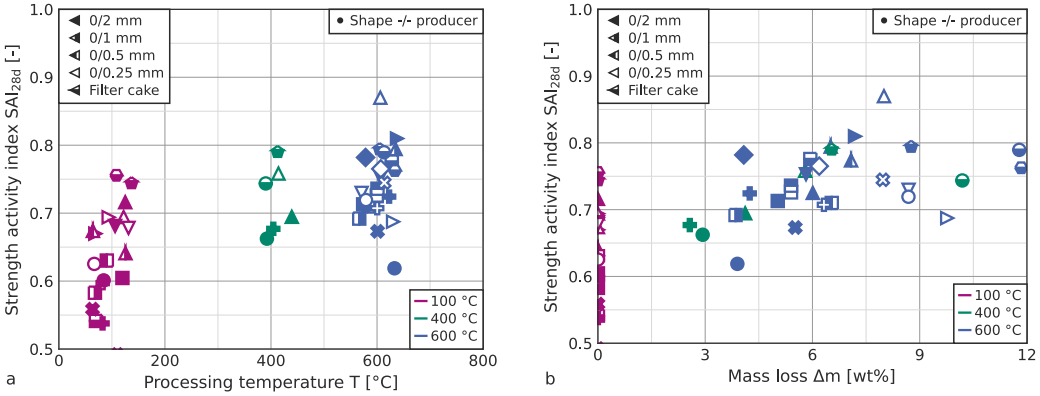

Fig. 9. Strength activity indices ($SAI_{28\,d}$) over processing temperatures (a) and mass loss (b) for different concrete fines at CEM I-substitution of $f = 0.3$ (see Table 1 for marker shapes). For better visualization only, results in (a) are randomly distributed around the activation temperatures of 100 °C, 400 °C, and 600 °C.

SAI for individual CEM I-series range between 0.95 and 1.05. While this uncertainty of the base mix strength is partially reflected in the scatter of SAI-results for processed concrete fines, the latter exhibit a high variation between different fines variations.

While investigating concrete fines from a single source, previous research found a logarithmic [63] or parabolic [49,64] relationship between processing temperature and compressive strength, or SAI, respectively. When applying the latter to the present data, the fit from Eq. (2) yields $SAI_0 = 0.59$, $SAI_1 = 5 \cdot 10^{-4}$, and $SAI_2 = -4 \cdot 10^{-7}$, albeit with a mediocre coefficient of variation ($R^2 = 0.44$)

$$SAI = SAI_0 + SAI_1 \cdot T + SAI_2 \cdot T^2 \qquad \text{with } SAI_{1,2,3}\text{: fit parameters} \tag{2}$$

When, instead of processing temperature, the relative mass loss during thermal activation is used as the horizontal axis, the bandwidth of the results for SAI reduces and shows a linear trend (see Fig. 9(b)). This can be expressed through Eq. (3), where the least squares method yields $SAI_n = 0.64$ and $SAI_m = 1.45$, with a slightly improved coefficient of determination ($R^2 = 0.47$).

$$SAI = SAI_n + SAI_m \cdot \Delta m \qquad \text{with } SAI_{n,m}\text{: fit parameters} \tag{3}$$

Due to the low coefficients of determination for both approaches, neither serves as a measure to predict compressive strength based on RCF properties or processing parameters. A more extensive, multipoint approach to account for the strength contribution of SCMs is the k-value concept as described in the European standard EN 206:2013, which uses these parameters to negate the impact of SCMs on relevant concrete properties, presently the compressive strength. The concept relies on the relationship between compressive strength and the water-cement ratio w/c, which is replaced through an equivalent water-cement ratio w/c_{eq} according

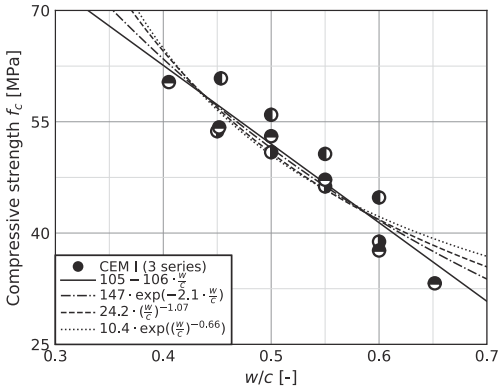

Fig. 10. Relationship between w/c and compressive strength f_c of base mixes without CEM I-substitution. Maker fill grades indicate results from three individual series.

to Eq. (4), where a concrete with partial cement substitution through an SCM has the same properties as a concrete without SCM with the same w/c-ratio.

$$\frac{w}{c_{\text{eq}}} = \frac{w}{c + k \cdot a} \qquad \text{with } a\text{: mass of the reactive SCM} \tag{4}$$

k-values serve as a measure of reactivity of the concrete additives and thus as an indication of their influence on compressive strength. Overall, k-values of a given SCM vary with concrete mix design, including water-cement ratio w/c and substitution rate. For most SCMs, k ranges between 0.0 and 1.0, where the former indicates an inert material, and the latter an SCM, which does not affect concrete properties when substituting CEM I.

The experimental determination of k-values uses the individual, mixture-dependent relationship between compressive strength f_c of mixtures without CEM I-substitution and the water-cement ratio w/c. For a mixture with SCMs, the equivalent water-cement ratio is then obtained by equating the resulting compressive strength with the relationship of w/c and f_c. Fig. 10 shows the individual results from three distinct series consisting of a total of 14 base mixes.

To represent the relationship mathematically, the experimental results were approximated by regression curves. Four approaches were examined for this purpose, which are shown in Fig. 10 with the respective optimized fit parameters (α_i, β_i).

$$f_{c,28\,\text{d}} = \alpha_1 - \beta_1 \cdot \frac{w}{c} \tag{5}$$

$$f_{c,28\,\text{d}} = \alpha_2 \cdot \exp\left(-\beta_2 \cdot \frac{w}{c}\right) \tag{6}$$

$$f_{c,28\,\text{d}} = \alpha_3 \cdot \left(\frac{w}{c}\right)^{-\beta_3} \tag{7}$$

$$f_{c,28\,\text{d}} = \alpha_4 \cdot \exp\left(\left[\frac{w}{c}\right]^{-\beta_4}\right) \tag{8}$$

The linear approach (Eq. (5)) – recommended in CEN/TR 16639:2014 – provides the best fit to the experimental results. Although linear material behavior is physically implausible, Eq. (6), Eq. (7), and Eq. (8) were discarded as empirical relationships for further analysis due to their insufficient fit. Furthermore, the comparison of the individual approaches illustrates that for mortar compressive strength between 43.4 MPa and 58.4 MPa, the linear approach yields higher values for w/c and thus lower values for k, corresponding to a conservative approach.

The subsequent determination of k calculates the individual equivalent water-cement ratio (Eq. (12)) and the respective k-value (Eq. (9)) for each mixture with the respective mixing parameters (w/b-ratio and cement substitution rate f) based on the compressive strength at the age of 28 d. The calculation of k requires additional input parameters such as the water-binder ratio w/b and the cement substitution rate f, as defined in Eq. (10) and (11).

$$k = \frac{1-f}{f} \cdot \left(\frac{\frac{w}{b}}{\frac{w}{z_{\text{eq}}}} \cdot \frac{1}{1-f} - 1 \right) = 1 + \frac{1}{f} \cdot \left(\frac{\frac{w}{b}}{\frac{w}{z_{\text{eq}}}} - 1 \right) \tag{9}$$

$$f = \frac{a}{b} = 1 - \frac{c}{b} \tag{10}$$

$$\frac{w}{b} = \frac{w}{c + a} \tag{11}$$

$$\frac{w}{c_{\text{eq}}} = \frac{\alpha_1 - f_{c,28\,\text{d}}}{\beta_1} \tag{12}$$

CEM I, by definition, has a k-value of $k = 1.0$. $k > 1.0$ can only be reached by highly reactive SCMS (as silica fume, according to EN 206:2013), where compressive strength increases when CEM I is substituted. Generally, the partial replacement of CEM I

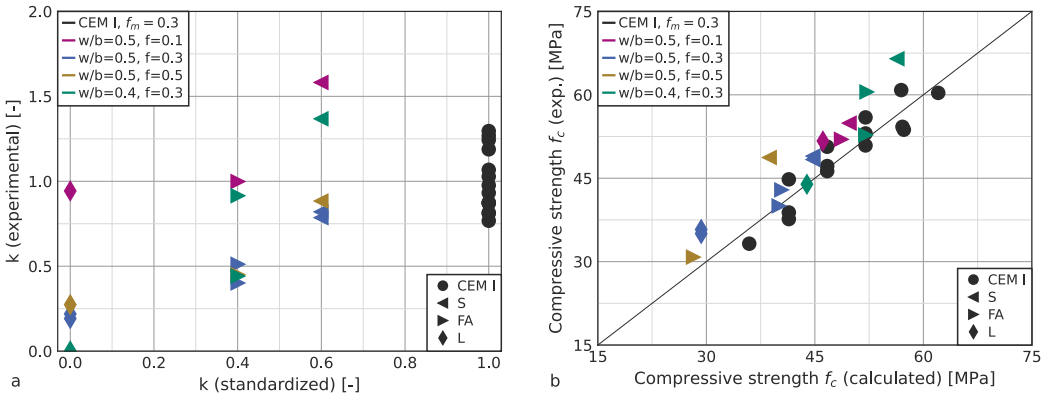

Fig. 11. a: k-values calculated for individual mortar mixes with CEM I substitution through established SCMs (slag (S), fly ash (FA), and limestone powder (L)) for different parameter combinations of the water-binder ratio w/b and the substitution rate f over respective design values in EN 206:2013.
b: measured compressive strength over calculated compressive strength using k from EN 206:2013.

Table 3
Average k-values for all processed RCF mixtures, clustered for different parameter combinations (excluding results from D-F-100 as outliers).

	100 °C	400 °C	600 °C	Total
$f = 0.1, w/b = 0.5$		0.20	0.61	0.51
$f = 0.3, w/b = 0.5$	0.17	0.36	0.39	0.30
$f = 0.3, w/b = 0.4$	0.01	0.40	0.43	0.26
$f = 0.3, w/b = 0.4/0.5$	0.09	0.38	0.41	0.28

through SCMs lowers compressive strength, which shows in $k < 1.0$. The magnitude of the strength reduction is represented by the value of k, where decreasing strength coincides with a reduction of k.

This behavior is exemplified by the reference SCMs (S, FA, and L) in Fig. 11. By definition in EN 206:2013, limestone powder (L) is an inert filler, consistent with $k = 0.0$, although slightly higher values for k have been proposed [80]. For $f = 0.3$, experimentally determined values for k range between 0.0 and 0.2. For fly ash and slag, experimental results in this study show a similar exceedance of conservative, standardized provisions, which are $k = 0.4$ for fly ash, and $k = 0.6$ for slag (EN 206:2013, CEN/TR 16639:2014). Experimental results yield $k = 0.4$–0.9 for fly ash and $k = 0.8$–1.4 for slag with $f = 0.3$, which reflects alternative standards and provisions [81,82]. For all tested SCMs, the substitution of 10 wt% of CEM I results in even higher k-values. However, when comparing the predicted compressive strength (by means of Eqs. (4) and (5)) to the experimentally measured compressive strength (Fig. 11(b)), this influence of the substitution rate f is mitigated. Nonetheless, f has a major influence on the scatter of k, which cannot be neglected for further analysis. Fig. 10 illustrates the three individual series for the determination of the fit parameters in Eq. (5). Between the different series, the measured strength has an apparent offset from the regression curve. The reason for this lies in deviating raw material properties, as the three series were produced with several months between them, so that all raw materials came from individual subsamples of the main batches. Fig. 11(b) compares these experimental results for CEM I to their prediction, which exhibits a similar scatter band as the reference SCMs, but lies around the bisector, while results for reference SCMs lie above. This is due to the aforementioned exceedance of standardized k-values, while $k = 1.0$ for CEM I is true by definition. Regardless, results for CEM I can be converted into individual k-values by assuming f in Eq. (9). For $f = 1.0$, k ranges between 0.9 and 1.0. This range increases hyperbolically with reducing f: For $f = 0.1$, the bandwidth of k for CEM I is 0.3 to 1.9, and for $f = 0.3$, k ranges between 0.8 and 1.3, with a standard deviation of 0.18.

For the second step of the analysis, 55 processed RCFs were used to produce 137 mortar mixtures, which were analyzed for their compressive strength and k-values. Generally, k-values increase with the processing temperature, whereby the difference between 400 °C and 600 °C is considerably smaller than the increase between 100 °C and 400 °C. The incorporation of RCFs processed at 100 °C can result in negative k-values, which is more pronounced for lower w/b-ratios. For 400 °C and 600 °C and the substitution rate $f = 0.3$, average k-values for different w/b-ratios deviate only slightly. Varying the substitution rate f at constant w/b has a higher, albeit ambiguous impact on k-values (see Table 3).

Fig. 12 shows the relationship between k-values calculated from the experimental results for $f = 0.3$ and the mass loss Δm during thermal processing. The RCFs in Fig. 12 were provided by the same manufacturer for each of the two upper diagrams. Batches A1 and A2, as well as B1 and B2, came from the same plants, so the same preparation technique for each pair can be assumed. However,

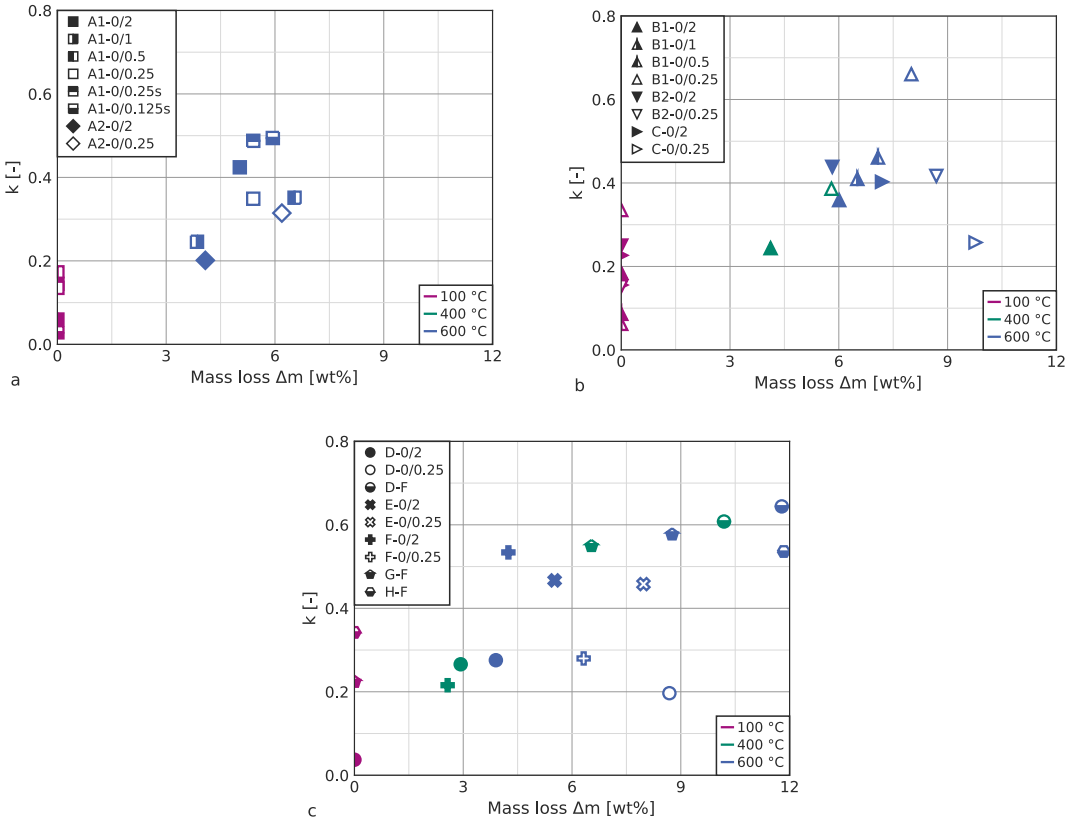

Fig. 12. k-values of select processed concrete fines over mass loss during thermal activation (averages for $w/b = 0.40$ and $w/b = 0.50$). Marker shapes and fill styles denote RCF producer and variation, and color indicates processing temperature.

the source concrete for A1 and A2, as well as B1 and B2, is for obvious reasons not the same, which includes different chemical compositions and mass losses. As mass loss also varies between variants of the same batch, a linear relationship between mass loss and k becomes apparent, notwithstanding scatter, especially for RCFs processed at 100 °C. Variants A1-0/0.25s and A1-0/0.125s, where the milling after the thermal activation was omitted, yielded higher k-values compared to milled variants at similar mass loss. Yet, this came with the side effect of impaired workability and higher superplasticiser demand, thus indicating an increased water demand. Two select variants from batch B1 were processed at 400 °C in addition to 100 °C and 600 °C, agreeing with the linear relationship between k and mass loss for batches B1 and B2.

Similar observations hold when considering the other RCF-variants illustrated in Fig. 12(c). Generally, RCFs processed at 400 °C yielded reduced mass losses and k-values compared to their 600 °C-counterparts. RCFs processed at 100 °C generally show low k-values, with some smaller than zero.

Variant D-F (filter cake from a fresh concrete recycling plant) showed the most noteworthy behavior: The RCF processed at 100 °C yielded a foam-like mortar with low density and low strength, resulting in $k = -0.55$, which is the lowest observed in this study. Mortars containing D-F-400 had a very stiff consistency, requiring the highest amount of superplasticizer within this study. However, the resulting k-values were among the highest, yet surpassed by D-F-600, which required less superplasticizer than its counterpart processed at 400 °C. Similar results for k were reached by other filter cake materials (G-F and H-F).

Subsequently, a linear model for the relationship between k and the mass loss Δm was fitted to the experimental results in Fig. 12 (Eq. (13)), excluding the variant D-F-100 as an outlier.

$$k = k_0 + k_m \cdot \Delta m k_0, \;\; k_m \text{ fit parameters} \tag{13}$$

Fit parameters k_0 and k_m were obtained through the least squares method. Predictably, $k_0 = 0.10$ roughly matches the average for RCFs processed at 100 °C (Table 3). $k_m = 4.55$ is based on direct mass loss measurements before and after thermal processing. These results, however, are possibly distorted by the decomposition of RCF components unrelated to hydration, such as organic material. The total organic carbon content (TOC) of the investigated RCFs ranges between 0.1 wt% (A2-0/2 and D-0/2) and 1.8 wt% (G-F).

Alternatively, the relevant mass loss can be obtained from thermogravimetric measurements, where the inert gas, in this case nitrogen (N_2), prevents the oxidation of carbons. By substituting Δm in Eq. (13) through the mass loss difference between

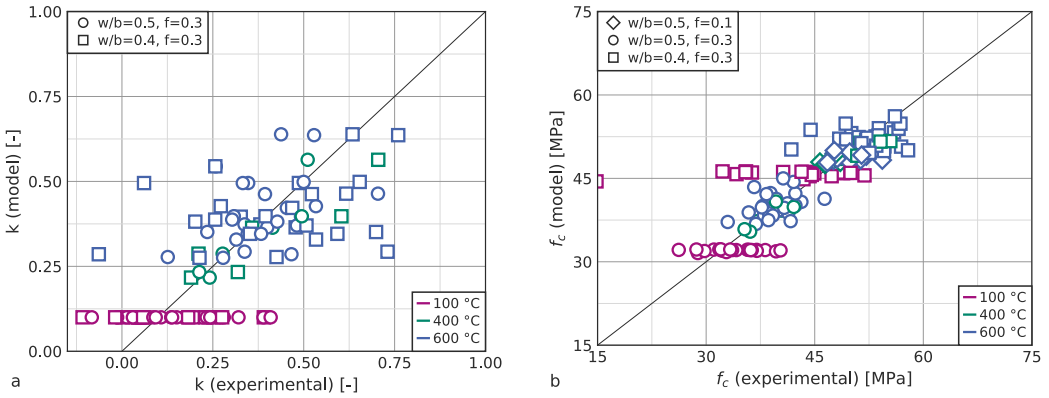

Fig. 13. Modeled k-values for a CEM I substitution rate through processed RCFs of $f = 0.3$ over k-values obtained from measurements (a) and modeled compressive strength over measured compressive strength (b). Marker shape indicates mix design, and color indicates activation temperature.

thermogravimetric measurements before and after thermal processing (Δm_{TG}), k_m increases to $k_{m,TG} = 5.30$. Eq. (15) provides an alternative interpretation of $k'_{m,TG}$. Under the assumption that Δm_{TG} comprises the total chemically bound water in cement hydration products, the parameter m_h illustrates the water consumption of one weight-unit of anhydrous cement. $k_{m,TG} = 5.30$ corresponds to $m_h = 0.23$, which agrees well with previous determinations of chemically bound water in OPC hydration products [83–85].

$$k = k_0 + k'_{m,TG} \cdot \Delta m_{TG} \tag{14}$$

$$= k_0 + \left(1 + \frac{1}{m_h}\right) \cdot \Delta m_{TG} \tag{15}$$

$$k_0,\ k'_{m,TG},\ m_h :\ \text{fit parameters} \tag{16}$$

Fig. 13 visualizes the individual comparison of the experimental results for compressive strength f_c and k versus their counterparts obtained from Eq. (13) in conjunction with Eq. (4) and (5). The coefficient of variation of the model for predicting k based on mass loss is mediocre with $R^2 = 0.60$. However, the scatter of the experimental and analytical results is to some extent due to the baseline scatter of the CEM I-series (compare Fig. 11). Consequently, the determination of the coefficient of determination for the extended model, which includes Eq. (5) for predicting compressive strength, yields an increase to $R^2 = 0.72$. This provides a significant improvement of the fit curve compared to SAI (Eq. (3)), even so, when only taking results for $w/b = 0.5$ and $f = 0.3$ into account, which yield $R^2 = 0.75$.

Table 4 lists the analysis of the model residuals $\Delta f_c = f_{c,\text{measured}} - f_{c,\text{modeled}}$ for different parameter combinations, which includes arithmetic means m and standard deviations s. For the reference SCMS (S, FA, and L), $m = 4.19$ means that measured compressive strength exceeds predicted compressive strength (based on k-valued from EN 206:2013) by more than 4 MPa, on average. For the base series with CEM I, and mortars including processed concrete fines, m is much smaller, since the model was fitted to the present data. The standard deviation of the residuals gives insight into the resulting deviations between measured strength results and the model, thereby allowing for a detailed analysis of the scatter. Since s for mixes containing processed concrete fines is higher than s for the CEM I base, the coefficient of variation cannot be completely explained through the scatter of CEM I. However, the present data imply this is mainly due to the high variations among RCFs processed at 100 °C. For RCFs, which were thermally activated, the residuals exhibit a lower scatter than the CEM I-mixes.

4. Conclusion and outlook

Thermal activation of recycled concrete fines (RCFs) is a promising procedure for construction and demolition waste recycling and CO_2-emission reduction as supplementary cementitious material (SCM). Industrial application requires a means for coping with variations in concrete fines composition. While usually focusing on a single precursor, comparing recent studies yields different strength activity indices (SAI), with processing temperature as the most important processing parameter.

The present study approaches this issue by processing 25 variations of 11 precursors and comparing their performance as SCM to reference materials, such as blast-furnace slag, fly ash, and limestone powder. Main findings include:

Table 4
Statistical parameters of the distribution of model residuals Δf_c for compressive strength. SCM: established SCMs (S, FA, L), f: substitution rate, T: activation temperature [°C], n: number of individual mortar mixes, m: arithmetic mean, and s: standard deviation directly calculated from Δf_c for the given parameter combinations.

	CEM I	SCM	RCF	RCF	RCF	RCF	RCF	RCF
f	–	0.3	0.3	0.3	0.1	0.3	0.1	0.3
T	–	–	all	100	400	400	600	600
n	14	10	103	41	7	12	23	50
m	−0.14	4.19	−0.18	−0.41	−0.87	0.65	1.07	−1.22
s	2.94	3.48	4.17	5.32	0.93	1.66	1.87	2.91

- Hydration heat development is accelerated and increased when CEM I is partially substituted through activated RCFs compared to reference SCMs like blast-furnace slag or fly ash. Subsequently, mortars containing processed concrete fines as SCM have a fast compressive strength development regardless of processing temperature, which is similar to CEM I and faster than fly ash or blast-furnace slag. This allows the application for structures, where fast demolding is required, e.g., in the precast industry.
- Compressive strength of mortar containing processed RCFs increases when RCFs are activated at 400 °C compared to processing at 100 °C. The positive influence of 600 °C over 400 °C is measurable, but smaller. Strength activity indices (SAI) from this study range from 0.67 to 0.81 (with two outliers) for 600 °C, and agree with findings in literature with regards to temperature dependence and scatter. Mass loss during processing is a better indicator for SAI, as RCFs with higher mass loss yield higher compressive strength.
- The present study proposes a model, which extends the k-value concept in the European standard EN 206:2013 for slag or fly ash. The compressive strength contribution of thermally processed RCFs with sufficiently high mass loss can exceed $k = 0.4$, which is the proposed k-value for fly ash, and even $k = 0.6$, which is applicable for slag.
- The determination of the mass loss of RCFs on samples in an inert atmosphere, e.g. in a thermogravimetric setup, provides a better agreement with theory, where k increases proportionally with the chemically bound water. This setup also allows for precursor screening and assessment before activation, where a lower boundary of the mass loss may serve as a compliance criterion.

However, the scatter of the obtained results underlines the necessity for additional research. The present study focuses on comparing thermally processed RCFs to established SCMs and proposing a simplified model approach for the strength contribution alongside existing provisions. The consideration of the influence of the chemical and mineralogical RCF composition may improve model accuracy for RCFs, where binder composition or aggregate reactivity varies. Besides, while the present study focuses on compressive strength development as a major concrete performance indicator, the influence of thermally activated RCFs on concrete long-term behavior requires additional research before practical application.

Furthermore, the presented model uses processed RCFs as a standalone SCM. Contemporary composite cements may consist of more than two different main constituents, which requires further development of the model. In the case of RCFs, blends with fly ash, slag, or nano silica have proven especially promising [51,53,67,86–92].

CRediT authorship contribution statement

Jan P. Höffgen: Writing – original draft, Visualization, Methodology, Funding acquisition, Formal analysis, Conceptualization. **Sebastian Bruckschlögl:** Writing – review & editing, Validation. **Bernhard Wetz:** Formal analysis. **Frank Dehn:** Writing – review & editing, Supervision, Project administration, Funding acquisition.

Declaration of Generative AI and AI-assisted technologies in the writing process

During the preparation of this work, the authors used Grammarly and DeepL in order to check for spelling and wording errors. After using these tools/services, the authors reviewed and edited the content as needed and take full responsibility for the content of the published article.

Funding

This work was supported by the Dres. Edith und Klaus Dyckerhoff-Stiftung, grant no. T0218/36374.

Declaration of competing interest

The authors declare that they have no known competing financial interests or personal relationships that could have appeared to influence the work reported in this paper.

Acknowledgments

The authors would like to thank Lukas Funk for his invaluable experimental work.

Appendix

See Fig. A.14 and Table A.5.

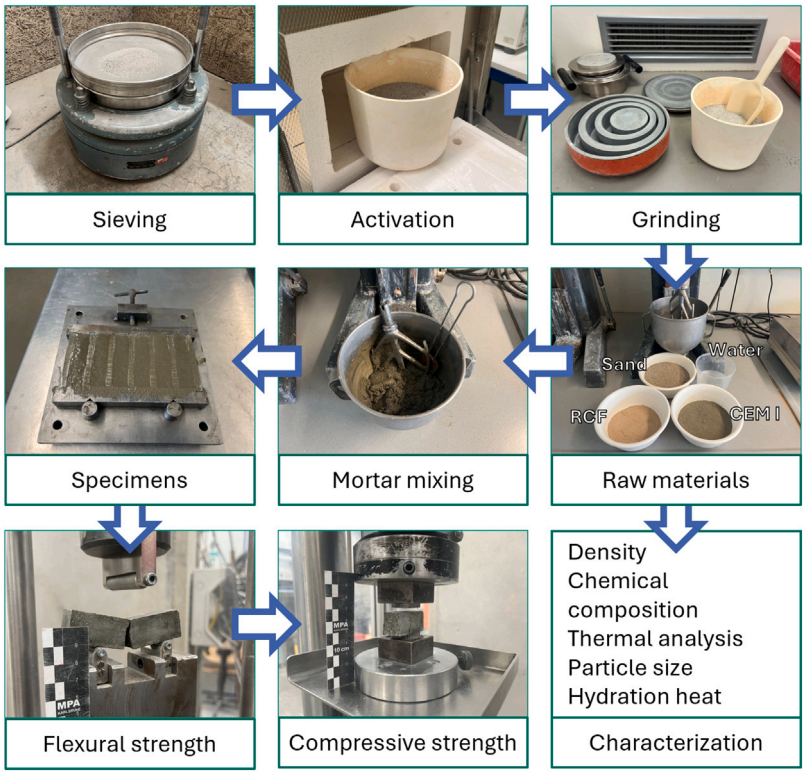

Fig. A.14. Graphical illustration of the experimental procedure.

Table A.5
Chemical composition and loss on ignition (LOI) of select RCF-variants (WDXRF in wt% according to EN 196-2:2013).

Variant	Na_2O wt%	MgO wt%	Al_2O_3 wt%	SiO_2 wt%	P_2O_5 wt%	K_2O wt%	CaO wt%	TiO_2 wt%	MnO wt%	Fe_2O_3 wt%	LOI wt%
A1-0/2	0.45	1.48	5.02	47.1	0.11	1.31	22.9	0.22	0.04	2.00	16.9
A1-0/0.25	0.48	1.64	5.48	45.2	0.12	1.33	23.1	0.25	0.04	2.22	17.4
A2-0/2	0.42	1.36	4.41	51.3	0.08	1.18	21.5	0.17	0.04	1.72	15.3
A2-0/0.25	0.41	1.72	5.10	43.1	0.10	1.19	23.4	0.22	0.05	2.10	21.2
B1-0/2	0.52	1.28	5.15	56.5	0.08	1.48	17.3	0.19	0.05	2.07	13.1
B1-0/0.25	0.51	1.49	5.48	49.0	0.10	1.44	20.4	0.22	0.05	2.19	16.2
B2-0/2	0.50	1.38	5.22	56.8	0.09	1.60	16.2	0.19	0.04	2.11	14.0
B2-0/0.25	0.52	1.86	5.99	47.7	0.10	1.63	19.7	0.25	0.05	2.37	17.3
C-0/2	0.50	1.73	5.34	56.8	0.09	1.44	15.1	0.19	0.07	1.80	14.3
C-0/0.25	0.51	2.51	6.23	45.5	0.11	1.45	19.2	0.25	0.10	2.10	19.1
D-0/2	0.61	0.76	4.36	71.7	0.05	1.11	10.5	0.18	0.03	1.08	7.3
D-0/0.25	0.73	1.41	6.04	54.1	0.09	1.22	18.9	0.34	0.05	1.79	13.2
D-F	0.43	1.86	5.84	42.7	0.09	0.76	25.1	0.27	0.06	1.60	17.6
E-0/2	0.51	1.22	5.21	51.5	0.10	1.44	19.7	0.20	0.04	1.82	15.4
E-0/0.25	0.50	1.63	6.37	42.9	0.14	1.40	23.3	0.28	0.05	2.33	18.4
F-0/2	0.63	0.94	5.27	56.3	0.10	1.61	17.4	0.21	0.04	1.75	13.7
F-0/0.25	0.70	0.91	5.23	56.7	0.10	1.58	16.7	0.22	0.05	1.78	13.9
G-F	0.70	2.02	7.23	41.1	0.15	1.46	21.9	0.31	0.10	3.31	19.8
H-F	0.34	1.65	6.00	32.7	0.22	1.07	27.8	0.26	0.04	2.72	23.3

Data availability

Data will be made available on request.

References

[1] M. Purton, Cement is a big problem for the environment. Here's how to make it more sustainable, 2024, https://www.weforum.org/stories/2024/09/cement-production-sustainable-concrete-co2-emissions/.

[2] Verein Deutscher Zementwerke, Environmental Data of the German Cement Industry 2023, Tech. rep., Düsseldorf, 2024.

[3] D. Coffetti, E. Crotti, G. Gazzaniga, M. Carrara, T. Pastore, L. Coppola, Pathways towards sustainable concrete, Cem. Concr. Res. 154 (2022) 106718, http://dx.doi.org/10.1016/j.cemconres.2022.106718.

[4] I.G. Richardson, The nature of the hydration products in hardened cement pastes, Cem. Concr. Compos. 22 (2) (2000) 97–113, http://dx.doi.org/10.1016/S0958-9465(99)00036-0.

[5] K.L. Scrivener, P. Juilland, P.J. Monteiro, Advances in understanding hydration of Portland cement, Cem. Concr. Res. 78 (2015) 38–56, http://dx.doi.org/10.1016/j.cemconres.2015.05.025.

[6] D.K. Panesar, R. Zhang, Performance comparison of cement replacing materials in concrete: Limestone fillers and supplementary cementing materials – A review, Constr. Build. Mater. 251 (2020) 118866, http://dx.doi.org/10.1016/j.conbuildmat.2020.118866.

[7] R. Snellings, P. Suraneni, J. Skibsted, Future and emerging supplementary cementitious materials, Cem. Concr. Res. 171 (2023) 107199, http://dx.doi.org/10.1016/j.cemconres.2023.107199.

[8] C. Orozco, S. Babel, S. Tangtermsirikul, T. Sugiyama, Comparison of environmental impacts of fly ash and slag as cement replacement materials for mass concrete and the impact of transportation, Sustain. Mater. Technol. 39 (2024) e00796, http://dx.doi.org/10.1016/j.susmat.2023.e00796.

[9] G.L. Golewski, Using digital image correlation to evaluate fracture toughness and crack propagation in the mode I testing of concretes involving fly ash and synthetic nano-SiO_2, Mater. Res. Express 11 (9) (2024) 095504, http://dx.doi.org/10.1088/2053-1591/ad755e.

[10] G.L. Golewski, Investigating the effect of using three pozzolans (including the nanoadditive) in combination on the formation and development of cracks in concretes using non-contact measurement method, Adv. Nano Res. 16 (3) (2024) 217–229, http://dx.doi.org/10.12989/ANR.2024.16.3.217.

[11] Y. Gao, G. Schutter, G. Ye, Z. Yu, Z. Tan, K. Wu, A microscopic study on ternary blended cement based composites, Constr. Build. Mater. 46 (2013) 28–38, http://dx.doi.org/10.1016/j.conbuildmat.2013.04.021.

[12] K.A. Knight, P.R. Cunningham, S.A. Miller, Optimizing supplementary cementitious material replacement to minimize the environmental impacts of concrete, Cem. Concr. Compos. 139 (2023) 105049, http://dx.doi.org/10.1016/j.cemconcomp.2023.105049.

[13] M. Barthel, K. Rübner, H.-C. Kühne, A. Rogge, F. Dehn, From waste materials to products for use in the cement industry, Adv. Cem. Res. 28 (7) (2016) 458–468, http://dx.doi.org/10.1680/jadcr.15.00149.

[14] F. Friol Guedes de Paiva, J.R. Tamashiro, L.H. Pereira Silva, A. Kinoshita, Utilization of inorganic solid wastes in cementitious materials – A systematic literature review, Constr. Build. Mater. 285 (2021) 122833, http://dx.doi.org/10.1016/j.conbuildmat.2021.122833.

[15] A. Carriço, J.A. Bogas, M. Guedes, Thermoactivated cementitious materials – A review, Constr. Build. Mater. 250 (2020) 118873, http://dx.doi.org/10.1016/j.conbuildmat.2020.118873.

[16] E.A. Ohemeng, S.O. Ekolu, A review on the reactivation of hardened cement paste and treatment of recycled aggregates, Mag. Concr. Res. 72 (10) (2020) 526–539, http://dx.doi.org/10.1680/jmacr.18.00452.

[17] L. Xu, J. Wang, K. Li, S. Lin, M. Li, T. Hao, Z. Ling, D. Xiang, T. Wang, A systematic review of factors affecting properties of thermal-activated recycled cement, Resour. Conserv. Recycl. 185 (2022) 106432, http://dx.doi.org/10.1016/j.resconrec.2022.106432.

[18] J.H. Aquino Rocha, R.D. Toledo Filho, The utilization of recycled concrete powder as supplementary cementitious material in cement-based materials: A systematic literature review, J. Build. Eng. 76 (2023) 107319, http://dx.doi.org/10.1016/j.jobe.2023.107319.

[19] Y. Zheng, X. Xi, H. Liu, C. Du, H. Lu, A review: Enhanced performance of recycled cement and CO2 emission reduction effects through thermal activation and nanosilica incorporation, Constr. Build. Mater. 422 (2024) 135763, http://dx.doi.org/10.1016/j.conbuildmat.2024.135763.

[20] R.V. Silva, J. Brito, R.K. Dhir, Properties and composition of recycled aggregates from construction and demolition waste suitable for concrete production, Constr. Build. Mater. 65 (2014) 201–217, http://dx.doi.org/10.1016/j.conbuildmat.2014.04.117.

[21] M. Nedeljković, J. Visser, B. Šavija, S. Valcke, E. Schlangen, Use of fine recycled concrete aggregates in concrete: A critical review, J. Build. Eng. 38 (2021) 102196, http://dx.doi.org/10.1016/j.jobe.2021.102196.

[22] S.K. Kaliyavaradhan, T.-C. Ling, K.H. Mo, Valorization of waste powders from cement-concrete life cycle: A pathway to circular future, J. Clean. Prod. 268 (2020) 122358, http://dx.doi.org/10.1016/j.jclepro.2020.122358.

[23] J. Li, X. Deng, Z. Lu, X. Li, L. Hou, J. Jiang, F. Yang, J. Zhang, K. He, Recycled concrete fines as a supplementary cementitious material: Mechanical performances, hydration, and microstructures in cementitious systems, Case Stud. Constr. Mater. 21 (2024) e03575, http://dx.doi.org/10.1016/j.cscm.2024.e03575.

[24] J.H.A. Rocha, R.D. Toledo Filho, Physical-mechanical assessment to mortars including recycled concrete powder and metakaolin, Case Stud. Constr. Mater. 21 (2024) e03996, http://dx.doi.org/10.1016/j.cscm.2024.e03996.

[25] Y. Yang, J. Xu, P. Gao, B. Zhan, Q. Yu, M. Ni, Y. Zhang, Study on the hydration characteristics and mechanical properties of recycled powder-slag powder-cement system, Case Stud. Constr. Mater. 21 (2024) e03952, http://dx.doi.org/10.1016/j.cscm.2024.e03952.

[26] T.F. Baggio, E. Possan, J.J. De Oliveira Andrade, Physical-chemical characterization of construction and demolition waste powder with thermomechanical activation for use as supplementary cementitious material, Constr. Build. Mater. 437 (2024) 136907, http://dx.doi.org/10.1016/j.conbuildmat.2024.136907.

[27] R. Baldusco, T.R.S. Nobre, S.C. Angulo, V.A. Quarcioni, M.A. Cincotto, Dehydration and rehydration of blast furnace slag cement, J. Mater. Civ. Eng. 31 (8) (2019) 04019132, http://dx.doi.org/10.1061/(ASCE)MT.1943-5533.0002725.

[28] S.C. Angulo, M.S. Guilge, V.A. Quarcioni, M.A. Cincotto, T.R. Nobre, H. Pöllmann, The role of calcium silicates and quicklime on the reactivity of rehydrated cements, Constr. Build. Mater. 340 (2022) 127625, http://dx.doi.org/10.1016/j.conbuildmat.2022.127625.

[29] J. Zelic, L. Ugrina, D. Jozic, Application of thermal methods in the chemistry of cement: kinetic analysis of portlandite from non-isothermal thermogravimetric data, in: The First International Proficiency Testing Conference, Sinaia, Romania, 2007, pp. 420–429.

[30] Q. Zhou, F.P. Glasser, Thermal stability and decomposition mechanisms of ettringite at <120°C, Cem. Concr. Res. 31 (9) (2001) 1333–1339, http://dx.doi.org/10.1016/S0008-8846(01)00558-0.

[31] Q. Zhou, E.E. Lachowski, F.P. Glasser, Metaettringite, a decomposition product of ettringite, Cem. Concr. Res. 34 (4) (2004) 703–710, http://dx.doi.org/10.1016/j.cemconres.2003.10.027.

[32] L.G. Baquerizo, T. Matschei, K.L. Scrivener, Impact of water activity on the stability of ettringite, Cem. Concr. Res. 79 (2016) 31–44, http://dx.doi.org/10.1016/j.cemconres.2015.07.008.

[33] J. Wang, L. Lacarrière, A. Sellier, Multicomponent modelling of cement paste dehydration under different heating rates, Mater. Struct. 52 (1) (2019) 6, http://dx.doi.org/10.1617/s11527-018-1306-9.

[34] I. Horváth, I. Proks, I. Nerád, Activation energies of the thermal decompositions of C3AH6 AND C3AD6 by the isothermal TG method, J. Therm. Anal. 12 (1) (1977) 105–110, http://dx.doi.org/10.1007/BF01909862.
[35] Z. He, X. Zhu, J. Wang, M. Mu, Y. Wang, Comparison of CO2 emissions from OPC and recycled cement production, Constr. Build. Mater. 211 (2019) 965–973, http://dx.doi.org/10.1016/j.conbuildmat.2019.03.289.
[36] V. Sousa, J.A. Bogas, Comparison of energy consumption and carbon emissions from clinker and recycled cement production, J. Clean. Prod. 306 (2021) 127277, http://dx.doi.org/10.1016/j.jclepro.2021.127277.
[37] S. Real, V. Sousa, I. Meireles, J.A. Bogas, A. Carriço, Life cycle assessment of thermoactivated recycled cement production, Mater. (Basel, Switzerland) 15 (19) (2022) http://dx.doi.org/10.3390/ma15196766.
[38] V. Sousa, J.A. Bogas, S. Real, I. Meireles, Industrial production of recycled cement: Energy consumption and carbon dioxide emission estimation, Environ. Sci. Pollut. Res. 30 (4) (2022) 8778–8789, http://dx.doi.org/10.1007/s11356-022-20887-7.
[39] V. Sousa, J.A. Bogas, S. Real, I. Meireles, A. Carriço, Recycled cement production energy consumption optimization, Sustain. Chem. Pharm. 32 (2023) 101010, http://dx.doi.org/10.1016/j.scp.2023.101010.
[40] J.A. Bogas, S. Real, A. Carriço, J. Abrantes, M. Guedes, Hydration and phase development of recycled cement, Cem. Concr. Compos. 127 (2022) 104405, http://dx.doi.org/10.1016/j.cemconcomp.2022.104405.
[41] C. Alonso, L. Fernandez, Dehydration and rehydration processes of cement paste exposed to high temperature environments, J. Mater. Sci. 39 (9) (2004) 3015–3024, http://dx.doi.org/10.1023/B:JMSC.0000025827.65956.18.
[42] P. Ge, Y. Song, J. Quan, Y. Wu, J. Zhou, Study on the activity, phase, thermal decomposition characteristics, microstructure, and chemical element of hardened cement powder under heating temperature of 100 °C~1200 °C, Struct. Concr. (2024) http://dx.doi.org/10.1002/suco.202301108, suco.202301108.
[43] N. Noel, T. Mielke, G. Semugaza, A.Z. Gierth, S. Helmich, S. Nawrath, D.C. Lupascu, Chemical transformations during the preparation and rehydration of reactivated virgin cements, Cement 19 (2025) 100129, http://dx.doi.org/10.1016/j.cement.2025.100129.
[44] E. Tajuelo Rodriguez, K. Garbev, D. Merz, L. Black, I.G. Richardson, Thermal stability of C-S-H phases and applicability of Richardson and Groves' and Richardson C-(A)-S-H(I) models to synthetic C-S-H, Cem. Concr. Res. 93 (2017) 45–56, http://dx.doi.org/10.1016/j.cemconres.2016.12.005.
[45] A. Carriço, S. Real, J.A. Bogas, M.F. Costa Pereira, Mortars with thermo activated recycled cement: Fresh and mechanical characterisation, Constr. Build. Mater. 256 (2020) 119502, http://dx.doi.org/10.1016/j.conbuildmat.2020.119502.
[46] S. Real, A. Carriço, J.A. Bogas, M. Guedes, Influence of the treatment temperature on the microstructure and hydration behavior of thermoactivated recycled cement, Materials 13 (18) (2020) 3937, http://dx.doi.org/10.3390/ma13183937.
[47] R. Serpell, F. Zunino, Recycling of hydrated cement pastes by synthesis of α'H-C2S, Cem. Concr. Res. 100 (2017) 398–412, http://dx.doi.org/10.1016/j.cemconres.2017.08.001.
[48] R. Yu, Z. Shui, Influence of agglomeration of a recycled cement additive on the hydration and microstructure development of cement based materials, Constr. Build. Mater. 49 (2013) 841–851, http://dx.doi.org/10.1016/j.conbuildmat.2013.09.004.
[49] X. Xi, Y. Zheng, C. Du, P. Zhang, M. Sun, Study on the hydration characteristics, mechanical properties, and microstructure of thermally activated low-carbon recycled cement, Constr. Build. Mater. 447 (2024) 138042, http://dx.doi.org/10.1016/j.conbuildmat.2024.138042.
[50] J.A. Bogas, A. Carriço, A.J. Tenza-Abril, Microstructure of thermoactivated recycled cement pastes, Cem. Concr. Res. 138 (2020) 106226, http://dx.doi.org/10.1016/j.cemconres.2020.106226.
[51] R. Serpell, M. Lopez, Properties of mortars produced with reactivated cementitious materials, Cem. Concr. Compos. 64 (2015) 16–26, http://dx.doi.org/10.1016/j.cemconcomp.2015.08.003.
[52] M. Wei, L. Chen, N. Lei, H. Li, L. Huang, Mechanical properties and microstructures of thermally activated ultrafine recycled fine powder cementitious materials, Constr. Build. Mater. 475 (2025) 141195, http://dx.doi.org/10.1016/j.conbuildmat.2025.141195.
[53] Z. Shui, D. Xuan, H. Wan, B. Cao, Rehydration reactivity of recycled mortar from concrete waste experienced to thermal treatment, Constr. Build. Mater. 22 (8) (2008) 1723–1729, http://dx.doi.org/10.1016/j.conbuildmat.2007.05.012.
[54] J.A. Bogas, A. Carriço, S. Real, Durability of concrete produced with recycled cement from waste concrete, Mater. Today: Proc. 58 (2022) 1149–1154, http://dx.doi.org/10.1016/j.matpr.2022.01.280.
[55] V. Letelier, E. Tarela, P. Muñoz, G. Moriconi, Combined effects of recycled hydrated cement and recycled aggregates on the mechanical properties of concrete, Constr. Build. Mater. 132 (2017) 365–375, http://dx.doi.org/10.1016/j.conbuildmat.2016.12.010.
[56] Z. Ma, J. Shen, H. Wu, P. Zhang, Properties and activation modification of eco-friendly cementitious materials incorporating high-volume hydrated cement powder from construction waste, Constr. Build. Mater. 316 (2022) 125788, http://dx.doi.org/10.1016/j.conbuildmat.2021.125788.
[57] D. Qian, R. Yu, Z. Shui, Y. Sun, C. Jiang, F. Zhou, M. Ding, X. Tong, Y. He, A novel development of green ultra-high performance concrete (UHPC) based on appropriate application of recycled cementitious material, J. Clean. Prod. 261 (2020) 121231, http://dx.doi.org/10.1016/j.jclepro.2020.121231.
[58] A. Tokareva, S. Kaassamani, D. Waldmann, Fine demolition wastes as supplementary cementitious materials for CO2 reduced cement production, Constr. Build. Mater. 392 (2023) 131991, http://dx.doi.org/10.1016/j.conbuildmat.2023.131991.
[59] P. Vashistha, Y. Oinam, H.-K. Kim, S. Pyo, Effect of thermo-mechanical activation of waste concrete powder (WCP) on the characteristics of cement mixtures, Constr. Build. Mater. 362 (2023) 129713, http://dx.doi.org/10.1016/j.conbuildmat.2022.129713.
[60] H. Wu, C. Liang, Z. Zhang, P. Yao, C. Wang, Z. Ma, Utilizing heat treatment for making low-quality recycled aggregate into enhanced recycled aggregate, recycled cement and their fully recycled concrete, Constr. Build. Mater. 394 (2023) 132126, http://dx.doi.org/10.1016/j.conbuildmat.2023.132126.
[61] J. Chen, J. Plank, Alkali-activated calcined clay blended cement: Effect of NaOH activator on performance of HPEG PCEs and on early strength, Cem. Concr. Res. 183 (2024) 107588, http://dx.doi.org/10.1016/j.cemconres.2024.107588.
[62] Z. He, R. Hu, Z. Ma, X. Liu, C. Wang, H. Wu, Reusing thermoactivated construction waste spoil as sustainable binder for durable concrete: Microstructure and chloride transport, Constr. Build. Mater. 398 (2023) 132553, http://dx.doi.org/10.1016/j.conbuildmat.2023.132553.
[63] J. Kim, N. Kim, Exploring the role of thermal activation of cement exposed to the external environment on the improvement of concrete properties, J. Mater. Res. Technol. 24 (2023) 2868–2878, http://dx.doi.org/10.1016/j.jmrt.2023.03.195.
[64] J. Kim, A. Ubysz, Thermal activation of multi-recycled concrete powder as supplementary cementitious material for repeated and waste-free recycling, J. Build. Eng. 98 (2024) 111169, http://dx.doi.org/10.1016/j.jobe.2024.111169.
[65] G. Semugaza, T. Mielke, M.E. Castillo, A.Z. Gierth, J.X. Tam, S. Nawrath, D.C. Lupascu, Reactivation of hydrated cement powder by thermal treatment for partial replacement of ordinary portland cement, Mater. Struct. 56 (3) (2023) http://dx.doi.org/10.1617/s11527-023-02133-9.
[66] Y. Sui, C. Ou, S. Liu, J. Zhang, Q. Tian, Study on properties of waste concrete powder by thermal treatment and application in mortar, Appl. Sci. 10 (3) (2020) 998, http://dx.doi.org/10.3390/app10030998.
[67] J. Wang, M. Mu, Y. Liu, Recycled cement, Constr. Build. Mater. 190 (2018) 1124–1132, http://dx.doi.org/10.1016/j.conbuildmat.2018.09.181.
[68] L. Xu, J. Wang, K. Li, T. Hao, Z. Li, L. Li, B. Ran, H. Du, New insights on dehydration at elevated temperature and rehydration of GGBS blended cement, Cem. Concr. Compos. 139 (2023) 105068, http://dx.doi.org/10.1016/j.cemconcomp.2023.105068.
[69] H. Zhang, B. Zhang, L. Tang, W. Zeng, Analysis of two processing techniques applied on powders from recycling of clay bricks and concrete, in terms of efficiency, energy consumption, and cost, Constr. Build. Mater. 385 (2023) 131517, http://dx.doi.org/10.1016/j.conbuildmat.2023.131517.
[70] E.W. Klingsch, Explosive Spalling of Concrete in Fire (Ph.D. thesis), ETH Zurich, Zürich, 2014, http://dx.doi.org/10.3929/ethz-a-010243000.
[71] H. Wu, D. Yang, Z. Ma, Micro-structure, mechanical and transport properties of cementitious materials with high-volume waste concrete powder and thermal modification, Constr. Build. Mater. 313 (2021) 125477, http://dx.doi.org/10.1016/j.conbuildmat.2021.125477.

[72] A. Lipowsky, A. Müller, Gesteinsmehl als Zuschlagstoffe in hydraulischen Bindemitteln, Aufbereitungs-Technik/Mineral Process. 58 (12) (2017) 52–64.
[73] L. Chen, M. Wei, N. Lei, H. Li, Effect of chemical–thermal activation on the properties of recycled fine powder cementitious materials, Case Stud. Constr. Mater. 20 (2024) e02956, http://dx.doi.org/10.1016/j.cscm.2024.e02956.
[74] M. Wei, L. Chen, N. Lei, H. Li, L. Huang, Experimental investigation on freeze–thaw resistance of thermally activated recycled fine powder concrete, Constr. Build. Mater. 457 (2024) 139378, http://dx.doi.org/10.1016/j.conbuildmat.2024.139378.
[75] D. Zhang, S. Zhang, B. Huang, Q. Yang, J. Li, Comparison of mechanical, chemical, and thermal activation methods on the utilisation of recycled concrete powder from construction and demolition waste, J. Build. Eng. 61 (2022) 105295, http://dx.doi.org/10.1016/j.jobe.2022.105295.
[76] J.A. Bogas, A. Carriço, M. Pereira, Mechanical characterization of thermal activated low-carbon recycled cement mortars, J. Clean. Prod. 218 (2019) 377–389, http://dx.doi.org/10.1016/j.jclepro.2019.01.325.
[77] K. Kalinowska-Wichrowska, M. Kosior-Kazberuk, E. Pawluczuk, The properties of composites with recycled cement mortar used as a supplementary cementitious material, Materials 13 (1) (2020) 64, http://dx.doi.org/10.3390/ma13010064.
[78] A. Carriço, S. Real, J.A. Bogas, Durability performance of thermoactivated recycled cement concrete, Cem. Concr. Compos. 124 (2021) http://dx.doi.org/10.1016/j.cemconcomp.2021.104270.
[79] S. Real, J.A. Bogas, A. Carriço, S. Hu, Mechanical characterisation and shrinkage of thermoactivated recycled cement concrete, Appl. Sci. 11 (6) (2021) 2454, http://dx.doi.org/10.3390/app11062454.
[80] C. Herget, A. Müller, T. Proske, M. Rezvani, C.-A. Graubner, Kalksteinmehl als Betonzusatzstoff – Vorschlag für die Anrechenbarkeit auf den Zementgehalt und Potenzial zur CO_2 -Reduktion im Betonbau, Beton- Und Stahlbetonbau 117 (2) (2022) 109–118, http://dx.doi.org/10.1002/best.202100073.
[81] W. Brameshuber, Sonderbetone für Tübbinge, in: R. Nothnagel, H. Twelmeier (Eds.), Baustoff Und Konstruktion, Springer Berlin Heidelberg, Berlin, Heidelberg, 2012, pp. 105–112, http://dx.doi.org/10.1007/978-3-642-29573-7.
[82] K. Weise, Die Reaktivität von Hüttensand als Betonzusatzstoff, Springer Fachmedien Wiesbaden, Wiesbaden, 2018, http://dx.doi.org/10.1007/978-3-658-20492-1.
[83] T.C. Powers, T.L. Brownyard, Studies of the physical properties of hardened portland cement paste, ACI J. Proc. 43 (9) (1946) 249–336, http://dx.doi.org/10.14359/15301.
[84] H. Brouwers, The work of powers and brownyard revisited: Part 1, Cem. Concr. Res. 34 (9) (2004) 1697–1716, http://dx.doi.org/10.1016/j.cemconres.2004.05.031.
[85] P. Lura, F. Winnefeld, X. Fang, A simple method for determining the total amount of physically and chemically bound water of different cements, J. Therm. Anal. Calorim. 130 (2) (2017) 653–660, http://dx.doi.org/10.1007/s10973-017-6513-z.
[86] L. Lu, Y. He, S. Hu, Binding materials of dehydrated phases of waste hardened cement paste and pozzolanic admixture, J. Wuhan Univ. Technol.-Mater. Sci. Ed. 24 (1) (2009) 140–144, http://dx.doi.org/10.1007/s11595-009-1140-6.
[87] R. Yu, Z. Shui, Efficient reuse of the recycled construction waste cementitious materials, J. Clean. Prod. 78 (2014) 202–207, http://dx.doi.org/10.1016/j.jclepro.2014.05.003.
[88] A. Yonis, Y. Oinam, P. Vashistha, A.B. Degefa, G.B. Belayneh, S. Park, S. Pyo, Novel activation method of waste concrete powder for sustainable clinker-free binder, Cem. Concr. Compos. 151 (2024) 105600, http://dx.doi.org/10.1016/j.cemconcomp.2024.105600.
[89] L. Zhang, J. Yongsheng, H. Guodong, J. Li, Y. Hu, Modification and enhancement of mechanical properties of dehydrated cement paste using ground granulated blast-furnace slag, Constr. Build. Mater. (164) (2018) 525–534, http://dx.doi.org/10.1016/j.conbuildmat.2017.12.232.
[90] Y. Jiang, Q. Ji, L. Feng, W. Luo, X. Wen, S. Chu, Ultra-green cement: Limestone calcined clay cement (LC3) with recycled cement, Cem. Concr. Compos. 163 (2025) 106210, http://dx.doi.org/10.1016/j.cemconcomp.2025.106210.
[91] X. Xi, Y. Zheng, J. Zhuo, P. Zhang, G.L. Golewski, C. Du, Influence of water glass modulus and alkali content on the properties of alkali-activated thermally activated recycled cement, Constr. Build. Mater. 452 (2024) 138867, http://dx.doi.org/10.1016/j.conbuildmat.2024.138867.
[92] X. Xi, Y. Zheng, J. Zhuo, P. Zhang, G.L. Golewski, C. Du, Mechanical properties and hydration mechanism of nano-silica modified alkali-activated thermally activated recycled cement, J. Build. Eng. 98 (2024) 110998, http://dx.doi.org/10.1016/j.jobe.2024.110998.